

Original Article



Mitochondrial Genome Editing: Exploring the Possible Relationship of the Atherosclerosis-Associated Mutation m.15059G>A With Defective Mitophagy

Vasily N. Sukhorukov ^{1,2,3,4,*} Victoria A. Khotina ^{1,2,*} Vladislav A. Kalmykov ^{1,2}
Alexander D. Zhuravlev ^{1,2} Vasily V. Sinyov ^{1,2,3} Daniil Y. Popov ⁴
Andrey Y. Vinokurov ⁴ Igor A. Sobenin ^{1,3} Alexander N. Orekhov ^{1,2,5}

¹Laboratory of Angiopathology, Institute of General Pathology and Pathophysiology, Moscow, Russia

²Laboratory of Cellular and Molecular Pathology of Cardiovascular System, Petrovsky National Research Centre of Surgery, Moscow, Russia

³Laboratory of Medical Genetics, Institute of Experimental Cardiology, Russian Medical Research Center of Cardiology, Moscow, Russia

⁴Cell Physiology and Pathology Laboratory of R&D Center of Biomedical Photonics, Orel State University, Orel, Russia

⁵Institute for Atherosclerosis Research, Moscow, Russia

OPEN ACCESS

Received: Oct 16, 2023

Revised: Nov 23, 2023

Accepted: Dec 19, 2023

Published online: Apr 18, 2024

Correspondence to

Victoria A. Khotina

Laboratory of Angiopathology, Institute of General Pathology and Pathophysiology, Baltiyskaya Street 4, Moscow 125315, Russia.
Email: nafany905@gmail.com

*Shared first authorship, worked together on the publication, and contributed equally.

© 2024 The Korean Society of Lipid and Atherosclerosis.

This is an Open Access article distributed under the terms of the Creative Commons Attribution Non-Commercial License (<https://creativecommons.org/licenses/by-nc/4.0/>) which permits unrestricted non-commercial use, distribution, and reproduction in any medium, provided the original work is properly cited.

ORCID iDs

Vasily N. Sukhorukov 

<https://orcid.org/0000-0002-0312-3773>

Victoria A. Khotina 

<https://orcid.org/0000-0003-2096-3237>

ABSTRACT

Objective: The aim of this study was to evaluate the effect of the m.15059G>A mitochondrial nonsense mutation on cellular functions related to atherosclerosis, such as lipodosis, pro-inflammatory response, and mitophagy. Heteroplasmic mutations have been proposed as a potential cause of mitochondrial dysfunction, potentially disrupting the innate immune response and contributing to the chronic inflammation associated with atherosclerosis.

Methods: The human monocytic cell line THP-1 and cytoplasmic hybrid cell line TC-HSMAM1 were used. An original approach based on the CRISPR/Cas9 system was developed and used to eliminate mitochondrial DNA (mtDNA) copies carrying the m.15059G>A mutation in the *MT-CYB* gene. The expression levels of genes encoding enzymes related to cholesterol metabolism were analyzed using quantitative polymerase chain reaction. Pro-inflammatory cytokine secretion was assessed using enzyme-linked immunosorbent assays. Mitophagy in cells was detected using confocal microscopy.

Results: In contrast to intact TC-HSMAM1 cybrids, Cas9-TC-HSMAM1 cells exhibited a decrease in fatty acid synthase (*FASN*) gene expression following incubation with atherogenic low-density lipoprotein. TC-HSMAM1 cybrids were found to have defective mitophagy and an inability to downregulate the production of pro-inflammatory cytokines (to establish immune tolerance) upon repeated lipopolysaccharide stimulation. Removal of mtDNA harboring the m.15059G>A mutation resulted in the re-establishment of immune tolerance and the activation of mitophagy in the cells under investigation.

Conclusion: The m.15059G>A mutation was found to be associated with defective mitophagy, immune tolerance, and impaired metabolism of intracellular lipids due to upregulation of *FASN* in monocytes and macrophages.

Keywords: Atherosclerosis; Mitochondria; Inflammation; Lipid metabolism; Mitophagy

Vladislav A. Kalmykov 
<https://orcid.org/0000-0002-9125-8538>
 Alexander D. Zhuravlev 
<https://orcid.org/0000-0002-0451-2594>
 Vasily V. Sinyov 
<https://orcid.org/0000-0001-5105-5763>
 Daniil Y. Popov 
<https://orcid.org/0000-0002-9436-1346>
 Andrey Y. Vinokurov 
<https://orcid.org/0000-0001-8436-1353>
 Igor A. Sobenin 
<https://orcid.org/0000-0003-0978-6444>
 Alexander N. Orekhov 
<https://orcid.org/0000-0002-3318-4681>

Funding

This study was funded by the Russian Science Foundation (grant #22-15-00064). The funding agency had no role in the design, collection, analysis, or interpretation of data; in the writing of the manuscript; or in the decision to submit the manuscript for publication.

Conflict of Interest

The authors have no conflicts of interest to declare.

Data Statement Availability

The datasets generated during and/or analyzed during the current study are available from the corresponding author on reasonable request.

Author Contributions

Conceptualization: Sukhorukov VN, Khotina VA; Data curation: Khotina VA, Kalmykov VA, Zhuravlev AD, Sinyov VV, Popov DY; Formal analysis: Khotina VA, Zhuravlev AD, Sinyov VV, Vinokurov AY; Writing - original draft: Sukhorukov VN, Khotina VA; Writing - review & editing: Sobenin IA, Orekhov AN.

INTRODUCTION

Atherosclerosis is a chronic disease characterized by localized inflammation within the walls of human arteries. The initial trigger for atherosclerosis development is the accumulation of intracellular lipids by intimal cells, resulting from the phagocytosis of modified low-density lipoprotein (LDL) particles.¹ Moreover, the phagocytosis of modified LDL can trigger a cellular pro-inflammatory response, which is part of the innate immune system. Disturbances in the innate immune response can result in chronic inflammation, which may ultimately lead to the development of an atherosclerotic lesion. Mitochondrial dysfunction is thought to be one of the causative factors of impaired innate immunity during atherosclerosis development. The presence of heteroplasmic mutations in mitochondrial DNA (mtDNA) can result in the emergence of dysfunctional mitochondria in intimal cells.² The primary mechanism for eliminating damaged mitochondria in cells is mitophagy, a process in which mitochondria merge with lysosomes for subsequent degradation.³ It has been established that certain mutations in mtDNA can disrupt the mitophagy process.^{4,5} Defective mitophagy allows damaged mitochondria to persist within cells, potentially triggering a chronic immune response,⁶ which contributes to the development of an atherosclerotic lesion accompanied by plaque formation.⁷

Our previous studies have identified several heteroplasmic mutations in mtDNA that are associated with atherosclerosis. These mutations were found to be present in atherosclerotic lesions within the human aortic intima.^{8,9} Specifically, mutations in the *MT-RNR1* (m.1555A>G), *MT-TL1* (m.3256C>T), *MT-TL2* (m.12315G>A), and mitochondrial cytochrome B (*MT-CYB*, m.15059G>A) genes were established to be associated with the formation of lipofibrous plaques in the intima of the human aorta.⁸ We have created cytoplasmic hybrid (cybrid) cell lines containing mitochondrial mutations associated with atherosclerosis in order to study the possible association between mutations in the mitochondrial genome and manifestations of atherosclerosis at the cellular level (e.g., the pro-inflammatory response and the accumulation of intracellular lipids).¹⁰ Using these cybrid cells, we have demonstrated the negative effect of mitochondrial mutations associated with atherosclerosis on the ability of cells to activate mitophagy and reduce the production of pro-inflammatory cytokines (leading to immune tolerance) in response to repeated lipopolysaccharide (LPS) stimulation.⁷ In summary, mitochondrial dysfunction, caused by a mitochondrial mutation, may provoke the accumulation of damaged mitochondria, leading to immune intolerance, non-resolving inflammation, and increased lipid accumulation in the cells of atherosclerotic plaques.

In this study, we investigated the effect of a mitochondrial mutation on lipidosis, the immune response, and mitophagy. Specifically, we focused on the role of the nonsense mutation m.15059G>A in the *MT-CYB*. This mutation results in the formation of a truncated cytochrome B protein, which can affect mitochondrial function. To eliminate mtDNA copies carrying the m.15059G>A mutation, we developed an original approach based on the CRISPR/Cas9 system. Using this approach, we successfully removed mtDNA carrying this target mutation and created cells that did not carry the m.15059G>A mutation (Cas9-TC-HSMAM1), based on the TC-HSMAM1 cybrid cell line. This made it possible to evaluate the effect of the m.15059G>A mutation, which may result in defective mitophagy and immune intolerance, on cellular metabolism and functions.

MATERIALS AND METHODS

1. MitoCas9 vector construction

The strategy of eliminating mtDNA from cybrid cells using a specific mitochondria-targeted CRISPR/Cas9 system was used in accordance with recent studies.^{14,13} A MitoCas9 vector was constructed that contained the full coding sequence of Sniper-Cas9 (*Streptococcus pyogenes*) with the flanking mitochondrial targeting sequence (MTS) of human cytochrome C oxidase subunit 8A and the T7 promoter sequence. The streptavidin-SpyTag sequence was added after the MTS site through the S1m aptamer for simultaneous delivery of Cas9 nuclease and single-guide RNA (sgRNA) into mitochondria.¹⁴ To increase the efficiency and specificity of mtDNA cutting with the MitoCas9 vector, biotinylated sgRNA was used. Site-specific mutagenesis with Sniper-Cas9 was performed to increase its stability and specificity, as previously described.^{15,18} The mtDNA-encoded gene *MT-CYB* with the m.15059G>A mutation was selected as a target for the MitoCas9 RNA complex.

2. Cell culture and transfection

The human monocytic cell line THP-1, as well as the cybrid cell line TC-HSMAM1 and Cas9-TC-HSMAM1 cells, was cultured in a complete culture medium of RPMI-1640 supplemented with L-glutamine, 10% (v/v) fetal bovine serum (FBS) (Gibco), 100 U/mL of penicillin-streptomycin (Gibco), and 50 mM β -mercaptoethanol (Sigma-Aldrich) at 37°C under a humidified atmosphere with 5% CO₂. THP-1 was used as a control (reference) cell line.

In total, 2.5×10^5 cells were seeded in a 24-well plate 24 hours prior to transfection. The MitoCas9 vector (1,000 ng) was transfected using mannose-containing cationic liposomes following an N/P ratio of 6:1, which represents the ratio of the number of amino groups in the cationic lipid to the number of phosphate groups in the nucleic acid.^{19,20} After 24 hours, the medium and liposomes were removed by washing the cells twice with phosphate-buffered saline (PBS).

3. Analysis of the efficiency of mitochondrial genome editing

For genomic DNA extraction, Cas9-TC-HSMAM1 cells were lysed overnight at 60°C in SNET lysis buffer (20 mM Tris, pH 8.0; 5 mM ethylenediaminetetraacetic acid [EDTA], pH 8.0; 400 mM NaCl; 1% sodium dodecyl sulfate) supplemented with proteinase K (20 mg/mL) (Sigma-Aldrich). Genomic DNA was purified using phenol:chloroform:isoamyl alcohol (25:24:1) according to the standard protocol.²¹ The DNA concentrations were determined using a BioSpec nano-spectrophotometer (Shimadzu). Extracted genomic DNA was used to amplify the surrounding region of the m.15059G>A mutation for the T7 endonuclease I (T7EI) mismatch detection assay using Q5 Hot Start High-Fidelity 2X Master Mix (New England BioLabs) in accordance with recent studies.²² Polymerase chain reaction (PCR) was conducted in a T100 thermal cycler (BioRad) in order to obtain PCR products. The purification and T7EI digestion of PCR products were carried out in accordance with the New England BioLabs protocol. Agarose gel electrophoresis of the digested PCR products was performed in the Sub Cell GT (BioRad) horizontal electrophoresis system. Gel imaging was carried out using the Gel Doc XR+ Gel Documentation System (BioRad). To confirm mtDNA cutting at the target site, we performed digital droplet PCR (ddPCR) on the PCR products isolated from agarose gel. Amplification was conducted using a QX200 (BioRad) with primers designed to detect double-strand DNA breaks (DSBs) in the region of heteroduplex formation after Cas9 endonuclease cleavage of the gene sequence (**Supplementary Table 1**). The number of events, corresponding to the fluorescent signals from cut mtDNA (positive) and wild-type mtDNA (negative), was quantified using QuantaSoft Analysis Pro software (BioRad).

4. Preparation of human plasma LDL

Plasma was obtained from patients with atherosclerosis and myocardial ischemia, consistent with the World Medical Association Declaration of Helsinki. Human LDL (density=1.019–1.063 g/cm³) was isolated by preparative sequential ultracentrifugation using KBr for density adjustments, according to standard techniques.^{23,24} To prevent lipoprotein oxidation, all steps were performed in the presence of 3 mM EDTA. The LDL preparations were dialyzed at 4°C in the dark against PBS containing 0.01 mM EDTA and sterilized through a polycarbonate filter with a 0.45 µm pore diameter (Corning Inc.). The protein content in LDL preparations was measured according to the method of Lowry et al.²⁵ using Folin-Ciocalteu's phenol reagent (Sigma-Aldrich). LDL preparations were stored in the dark at 4°C for 7 days until use.

5. Generation of macrophage foam cells and measurement of their cellular cholesterol content

THP-1, TC-HSMAM1, and Cas9-TC-HSMAM1 cells were maintained in a complete RPMI-1640 medium and 100 ng/mL of phorbol 12-myristate-13-acetate (Sigma-Aldrich) at 37°C for 48 hours to induce cell differentiation to macrophages.²⁶ Cell-derived macrophages were incubated in the presence of previously isolated LDL (100 µg/mL) for 24 hours to induce lipid accumulation and foam cell formation. To measure cellular cholesterol content, the cells were lysed in a 0.2N sodium hydroxide solution, and the protein levels in the cellular lysates were then measured according to the method of Lowry et al.,²⁵ using 1 mg/mL bovine serum albumin as a standard. Cellular lipids were extracted from cell samples using hexane–isopropanol (3:2; v/v). Cholesterol levels in the lipid extracts were measured using Fluitest CHOL (Analyticon) and a 1 mg/mL cholesterol solution as a standard. The total cholesterol content was calculated as the ratio of cholesterol to cell protein in each sample.

6. Analysis of gene expression for lipid metabolism enzymes

Quantitative real-time PCR (qPCR) was used to analyze the expression levels of selected genes that encode enzymes involved in cholesterol metabolism in non-loaded and cholesterol-loaded macrophages. Total cellular RNA was isolated using the ExtractRNA (Evrogen) with the removal of genomic DNA using the ezDNase Enzyme (Invitrogen) according to the manufacturer's protocol. RNA concentrations were determined using a BioSpec nanospectrophotometer (Shimadzu). The RNA from each sample was then converted to cDNA using an MMLV RT kit (Evrogen) according to the manufacturer's protocol. cDNAs from samples were amplified in triplicate with CFX96 Touch (BioRad) using the qPCRmix-HS SYBR (Evrogen) for qPCR using designed primers (**Supplementary Table 2**). The data were normalized relative to the median Ct values of endogenous controls (*GAPDH* and *CAP1*). The fold difference between the THP-1 control and treatments was calculated using the $2^{-\Delta\Delta Ct}$ method, where $\Delta\Delta Ct = (\Delta Ct \text{ THP-1 control}) - (\Delta Ct \text{ treatment})$ and $\Delta Ct = (Ct \text{ target gene}) - (\text{median Ct value of the endogenous control})$.

7. Evaluation of tumor necrosis factor (TNF)-α secretion of LPS-stimulated cells using enzyme-linked immunosorbent assay (ELISA)

THP-1, TC-HSMAM1, and Cas9-TC-HSMAM1 cells were maintained in a complete RPMI-1640 medium supplemented with 10% FBS and 1 µg/mL LPS from *Escherichia coli* O111:B4 (Sigma-Aldrich) at 37°C for 16 hours (first LPS hit) to induce a pro-inflammatory response.²⁷ After incubation, the samples were centrifuged at 200 × g for 10 minutes and washed with PBS. The supernatant was removed, and fresh complete RPMI-1640 medium supplemented with 10% FBS with or without 1 µg/mL LPS was added to the cells for additional incubation

for 4 hours (second LPS hit). Next, cell culture medium from each sample was aspirated and centrifuged at $200 \times g$ for 10 minutes. The supernatants were used for subsequent analyses. The concentration of TNF- α in the supernatants was determined using a TNF- α ELISA Kit (R&D Systems) and Nunc MaxiSorp ELISA Plates (Thermo Fisher Scientific) following the manufacturer's protocol. Absorbance was measured at 495 nm using an AMR-100T microplate reader (Allsheng).

8. Mitochondrial membrane potential measurement

The mitochondrial membrane potential ($\Delta\Psi_m$) was estimated using tetramethylrhodamine methyl ester (TMRM) (Ex/Em 551/578) (Invitrogen) with an epifluorescence inverted microscope. Fluorescence was excited by a xenon arc lamp with a monochromator (550 \pm 10 nm) and recorded after passing through a filter with a bandwidth of 575–630 nm (Cairn Research) using a cooled sCMOS camera (Teledyne Photometrics). Briefly, 1×10^6 cells were washed twice with Hank's balanced salt solution (HBSS) and loaded with 25 nM TMRM in HBSS for 45 minutes without subsequent washing. To determine the mechanism of $\Delta\Psi_m$ maintenance, oligomycin A (2 μ g/mL) (Sigma-Aldrich), rotenone (2 μ M) (Sigma-Aldrich), and carbonyl cyanide 4-(trifluoromethoxy)phenylhydrazone (FCCP) (2 μ M) (Sigma-Aldrich) were added during fluorescence intensity recording.²⁸

9. Detection of mitophagy in cells using confocal microscopy and qPCR

THP-1, TC-HSMAM1, and Cas9-TC-HSMAM1 cells were cultured in complete RPMI-1640 medium on a 6-well plate. Mitochondria were stained with 100 nM MitoTracker Green (Invitrogen) for 30 minutes at room temperature. The cells were then incubated for 6 hours at 37°C under a humidified atmosphere with 5% CO₂ in the presence of 5 μ M FCCP (Sigma-Aldrich) to induce mitophagy. Next, the lysosomes were stained with 50 nM LysoTracker Deep Red (Invitrogen) for 30 minutes at room temperature. After that, the cells were transferred to confocal dishes. The images were captured on a Leica DMI8 STELLARIS 5 confocal microscope (Leica Microsystems) with an HC PL APO CS2 63x/1.40 OIL objective. Some of the cell samples were utilized for RNA isolation, followed by real-time PCR and qPCR to analyze the expression of genes associated with the activation of both the canonical and non-canonical mitophagy pathways, employing primers designed for this purpose (**Supplementary Table 2**).

10. Statistical analysis

All experiments were performed in triplicate to confirm the reproducibility of the results. IBM SPSS Statistics 27.0.1 software (IBM Corp.) was used to analyze the data. The normality of the data distribution was tested with the Shapiro-Wilk or Kolmogorov-Smirnov tests. The Student's *t*-test was used for comparisons between 2 groups when the data distribution was normal. If the data distribution was non-normal, the Mann-Whitney *U* test was used. For comparisons of more than 2 groups, one-way analysis of variance adjusted with the Bonferroni correction was employed if the data distribution was normal. If the data distribution was non-normal, the Kruskal-Wallis test adjusted with the Bonferroni correction was used for comparisons of more than 2 groups. The results of relative gene expressions, cytokine secretion, and normalized mitophagy levels are shown as the means \pm standard deviation. The captured confocal images were assessed using the CellProfiler software (Broad Institute of MIT and Harvard). The level of significance was set to $p < 0.05$. Data visualizations for ddPCR analysis, relative gene expressions, cytokine secretion, and normalized mitophagy levels were prepared using GraphPad Prism 8 software (GraphPad Software Inc.).

RESULTS

1. Elimination of m.15059G>A mutation in the MT-CYB gene by MitoCas9 RNA complex

We developed a method to eliminate the m.15059G>A mutation from the mitochondrial genome using the MitoCas9 RNA complex to target and remove all mtDNA copies carrying this mutation (Fig. 1A). The efficiency of cell transfection and elimination of mtDNA containing the m.15059G>A mutation was assessed using ddPCR with primers that detected DSBs at the region of heteroduplex formation after Cas9 endonuclease-mediated gene cleavage. The cutting of mtDNA at the site of the m.15059G>A mutation was confirmed using the T7EI mismatch detection assay (Fig. 1B). As a result, the heteroplasmy level of the m.15059G>A mutation was reduced from 79.29%±11.58% to 12.81%±3.24% ($p<0.001$) in TC-HSMAM1 cybrids treated with the MitoCas9 RNA complex (Fig. 1C).

Thus, we showed that the MitoCas9 RNA complex can effectively induce DSBs in the *MT-CYB* gene carrying the m.15059G>A pathogenic mutation in TC-HSMAM1 cytoplasmic hybrids. This approach allowed us to minimize the heteroplasmy level of the m.15059G>A mutation.

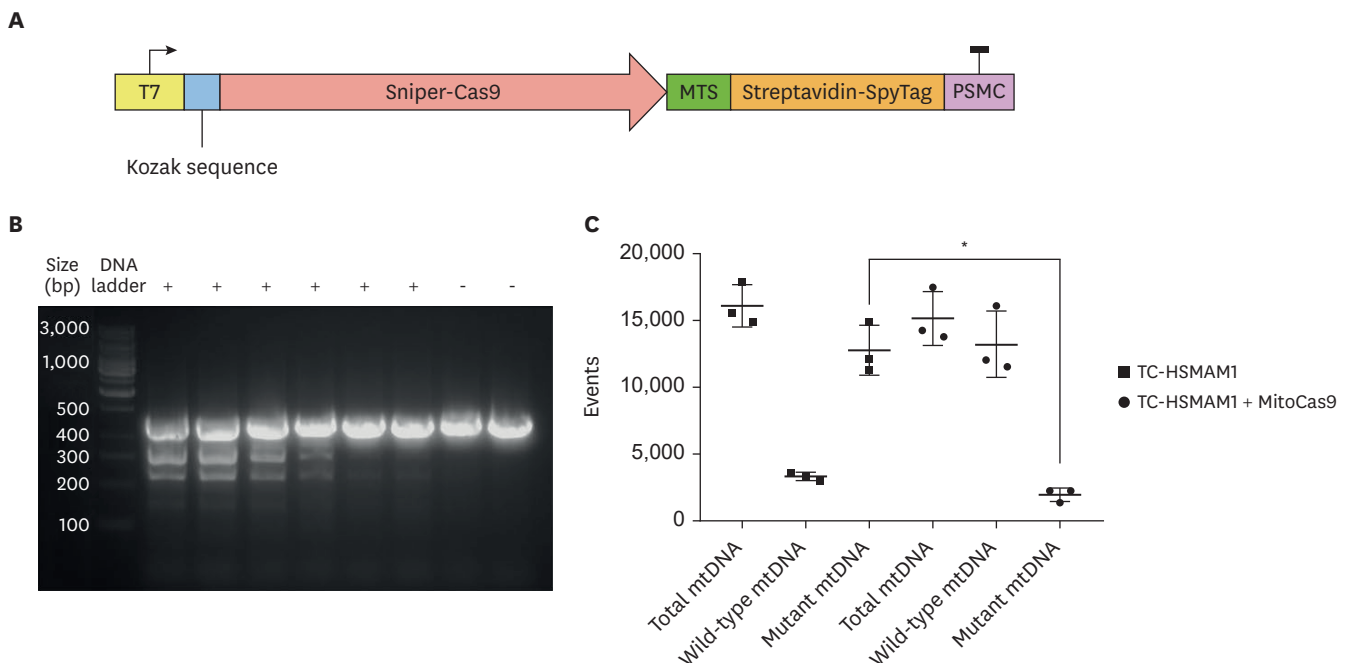


Fig. 1. Elimination of the m.15059G>A mutation in the mitochondrial cytochrome B gene by MitoCas9 RNA complex. (A) The MitoCas9 vector structure. (B) Representative gel image of T7EI-treated PCR products amplified from mtDNA with the m.15059G>A mutation. The T7EI method showed that heteroduplexes were identified in the 6 elevated regions by PCR, indicating that the MitoCas9 RNA complex cleaved the double-stranded mtDNA at the target site. Moreover, no T7EI cleavage was observed in 2 negative controls with PCR products amplified from cell mtDNA, where the MitoCas9 RNA complex was not applied. (+): PCR products amplified from the mtDNA with the m.15059G>A mutation, where the cleavage was found. (-): PCR products amplified from wild-type mtDNA, where the cleavage was not found. (C) Efficacy of elimination of mtDNA with the m.15059G>A mutation by the MitoCas9 RNA complex. T7EI, T7 endonuclease I; T7, T7 promoter sequence; PCR, polymerase chain reaction; mtDNA, mitochondrial DNA; Sniper-Cas9, Cas9 coding sequence; MTS, mitochondrial targeting sequence derived from the cytochrome c oxidase subunit 8A sequence; Streptavidin-SpyTag, streptavidin/biotin; PSMC, terminator region; Wild-type mtDNA, intact mtDNA without mutation; Mutant mtDNA, mtDNA carrying the m.15059G>A mutation in mitochondrial cytochrome B gene; Total mtDNA, the total number of mtDNA copies; TC-HSMAM1, cybrid cells without transfection with MitoCas9 RNA complex; TC-HSMAM1 + MitoCas9, TC-HSMAM1 cells treated by the MitoCas9 RNA complex. Data information: * $p<0.001$ (Mann-Whitney *U* test).

2. The m.15059G>A mutation can potentially affect intracellular lipid metabolism by altering the expression of the *FASN* gene

To assess the role of m.15059G>A in the intracellular cholesterol accumulation, THP-1, TC-HSMAM1, and Cas9-TC-HSMAM1 cells were incubated with LDL isolated from the blood of patients with atherosclerosis (atherogenic LDL). The initial content of total cholesterol was found to be similar across all studied cell lines (Fig. 2A). However, when control THP-1 cells were incubated with LDL from atherosclerotic patients, there was a 1.15-fold increase in cholesterol content ($p<0.01$), highlighting the atherogenic properties of LDL in native cell culture. Additionally, incubation of TC-HSMAM1 and Cas9-TC-HSMAM1 cells with

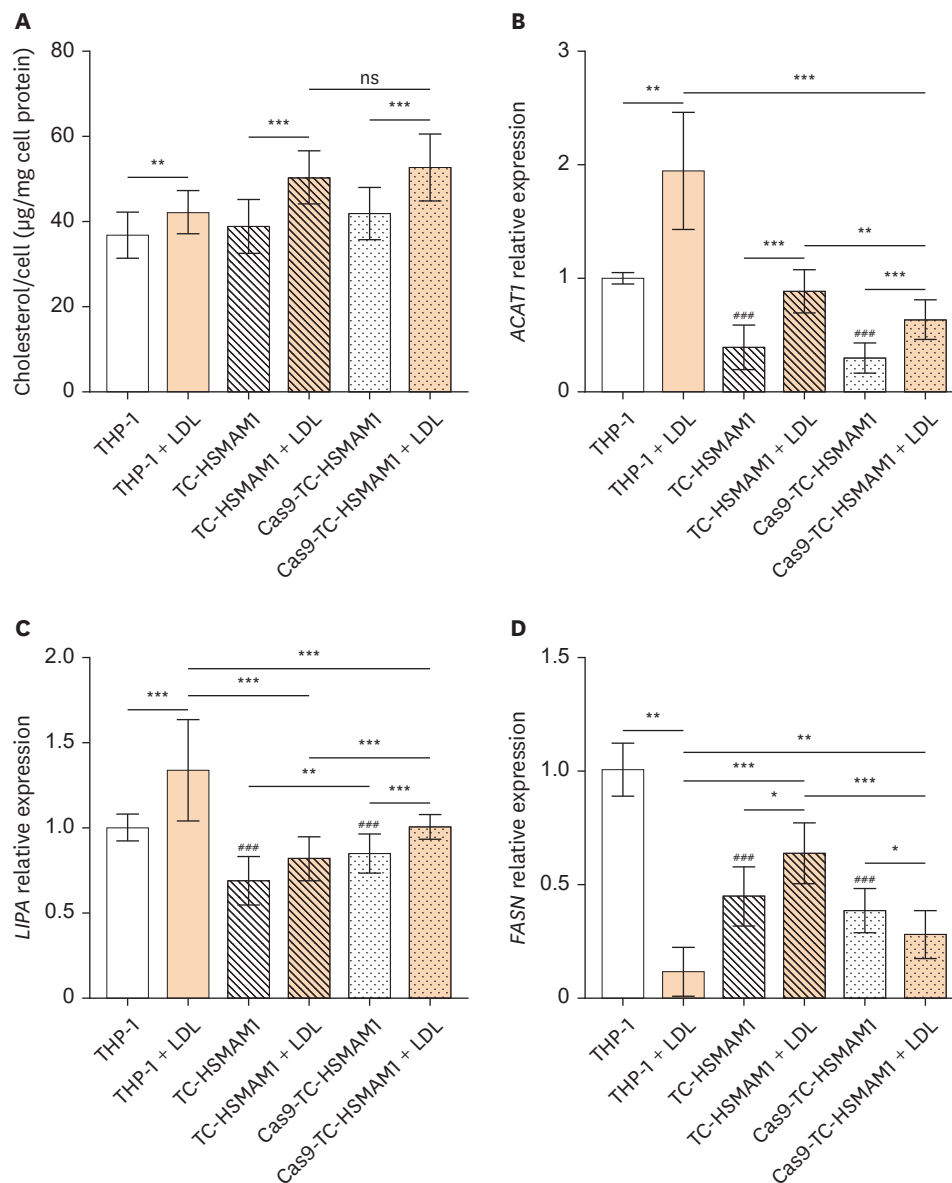


Fig. 2. Evaluation of lipid metabolism in THP-1, TC-HSMAM1, and Cas9-TC-HSMAM1 cells. (A) Total cholesterol levels of PMA-differentiated THP-1, TC-HSMAM1, and Cas9-TC-HSMAM1 cells. (B) Relative expression of the *ACAT1* gene. (C) Relative expression of the *LIPA* gene. (D) Relative expression of the *FASN* gene. Data information: bars are mean \pm standard deviation. ns, not significant; LDL, low-density lipoprotein; PMA, phorbol 12-myristate-13-acetate; *ACAT1*, acetyl-CoA acetyltransferase 1; *LIPA*, lysosomal acid lipase; *FASN*, fatty acid synthase; TC-HSMAM1, cybrid cells without transfection with MitoCas9 RNA complex. ns ($p>0.05$), * $p<0.05$, ** $p<0.01$, *** $p<0.001$, **** $p<0.001$ vs. THP-1 (one-way analysis of variance adjusted with the Bonferroni correction).

atherogenic LDL led to a significant increase in total cholesterol levels by 1.29-fold ($p < 0.001$) and 1.26-fold ($p < 0.001$), respectively, compared to cells not incubated with LDL. Despite this, there was no significant difference in total cholesterol levels between the 2 cybrid cell lines incubated with atherogenic LDL. The lack of a significant effect on cholesterol accumulation in cybrid cells following the elimination of mtDNA suggests that the m.15059G>A mutation in the *MT-CYB* gene does not substantially influence intracellular cholesterol accumulation. Intracellular lipid metabolism was evaluated using real-time PCR to measure the relative gene expression of key enzymes involved in lipid metabolism: acetyl-CoA acetyltransferase 1 (*ACAT1*), which is responsible for the formation of acetoacetyl-CoA; lysosomal acid lipase (*LIPA*), also known as cholesterol ester hydrolase, which catalyzes the hydrolysis of cholesterol esters and triglycerides within lysosomes; and fatty acid synthase (*FASN*), which is involved in the synthesis of saturated fatty acids (**Fig. 2B-D**). We observed that the basal gene expression levels of *ACAT1*, *LIPA*, and *FASN* were downregulated in TC-HSMAM1 and Cas9-TC-HSMAM1 cells compared to the control THP-1 cells ($p < 0.001$). Furthermore, there was no significant difference in the basal gene expression of these key enzymes in lipid metabolism between TC-HSMAM1 and Cas9-TC-HSMAM1 cells, except for *LIPA*, which showed increased expression in Cas9-TC-HSMAM1 cells ($p < 0.01$).

In THP-1 cells incubated with atherogenic LDL, there was an increase in *ACAT1* and *LIPA* gene expression ($p < 0.01$ and $p < 0.001$, respectively), while *FASN* gene expression decreased ($p < 0.01$) compared to cells not incubated (basal gene expression). In TC-HSMAM1 cybrids treated with LDL, there was an observed increase in *ACAT1* ($p < 0.001$) and *FASN* ($p < 0.05$) gene expression relative to the basal expression, whereas *LIPA* gene expression remained unchanged. In Cas9-TC-HSMAM1 cells incubated with LDL, there was an increase in *LIPA* and *ACAT1* gene expression ($p < 0.001$) and a decrease in *FASN* gene expression ($p < 0.05$) when compared to the basal gene expression (**Fig. 2D**).

Taken together, the data on the expression of the key enzymes of lipid metabolism and the content of cholesterol in cybrids before and after the elimination of the proatherogenic mutation support the conclusion that the m.15059G>A mutation can affect intracellular lipid metabolism by changing the expression of the *FASN* gene. It is interesting to note that the expression of this gene in Cas9-TC-HSMAM1 cells decreases in response to LDL, since the cells do not require *de novo* synthesized fatty acids in the presence of a source of exogenous fatty acids. However, this reduction in *FASN* expression was not observed in cybrids harboring the m.15059G>A mutation.

3. The m.15059G>A mutation may contribute to the inability of monocyte-like cells to form innate immune tolerance

The ability of intact THP-1, TC-HSMAM1, and Cas9-TC-HSMAM1 cells to form immune tolerance in response to pro-inflammatory stimulation with bacterial LPS was evaluated using ELISA (**Fig. 3**). Secretion of the pro-inflammatory cytokine TNF- α was measured after the first and second stimulation of cells with LPS (i.e., LPS hits).

An increase in TNF- α secretion in response to initial LPS stimulation, followed by an absence of this effect upon subsequent stimulation, was demonstrated in control THP-1 cells (**Fig. 3**). Consequently, these control cells were capable of developing immune tolerance. In contrast, TC-HSMAM1 cybrids harboring the m.15059G>A mutation exhibited an inability to establish immune tolerance in response to LPS stimulation, as evidenced by sustained TNF- α secretion upon repeated LPS challenges. Notably, TNF- α secretion following the second LPS

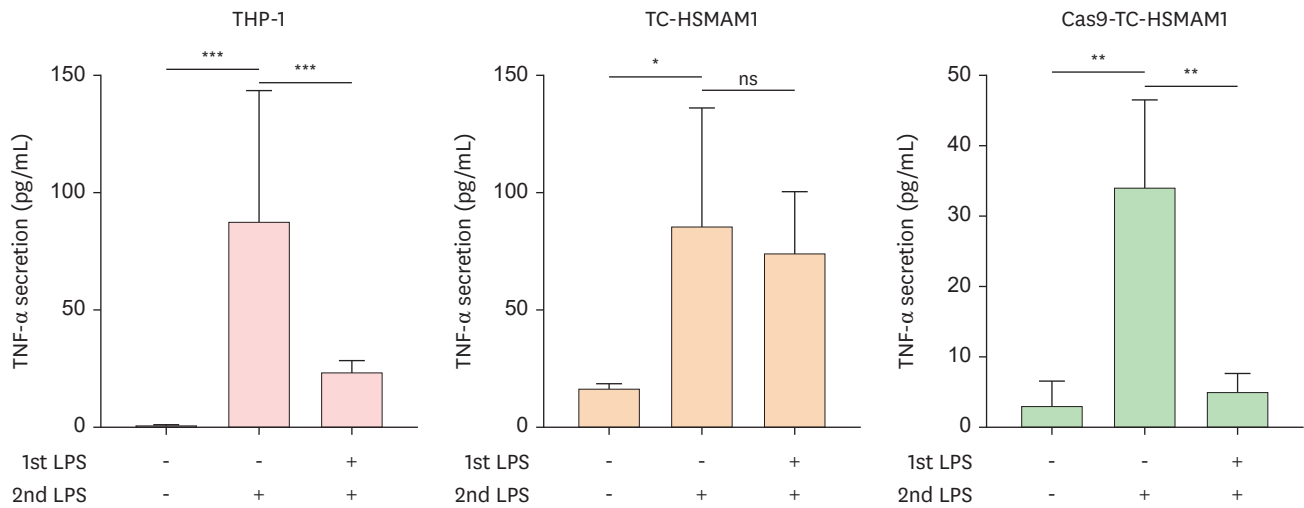


Fig. 3. Innate immune tolerance of THP-1, TC-HSMAM1, and Cas9-TC-HSMAM1 cells. The 1st LPS: LPS stimulation for 16 hours. The 2nd LPS: LPS stimulation for 4 hours. (-): no stimulation. (+): LPS stimulation. Data information: bars are mean \pm standard deviation. ns, not significant; LPS, lipopolysaccharide; TNF, tumor necrosis factor; TC-HSMAM1, cybrid cells without transfection with MitoCas9 RNA complex. ns ($p>0.05$), * $p<0.05$, ** $p<0.01$, *** $p<0.001$ (one-way analysis of variance adjusted with the Bonferroni correction).

stimulation was significantly reduced ($p<0.01$) in Cas9-TC-HSMAM1 cells compared to the secretion after the initial stimulation, indicating a restoration of immune tolerance in these cells. Therefore, the m.15059G>A mutation was identified as having a detrimental impact on the immune tolerance of monocytes, thereby impeding the resolution of inflammation.

4. The m.15059G>A mutation has the potential to disrupt PTEN-induced kinase (PINK)/Parkin-mediated mitophagy and impair the function of complex I

$\Delta\Psi_m$ serves as a crucial indicator of mitochondrial health. The change in TMRM fluorescence intensity between basal and fully depolarized states can be used to assess $\Delta\Psi_m$ (Fig. 4A). After the removal of mutated mtDNA, there was a significant 43.5% increase in $\Delta\Psi_m$ levels in Cas9-TC-HSMAM1 cells compared to THP-1 cells ($p=0.001$). However, there was no statistically significant difference in $\Delta\Psi_m$ levels between Cas9-TC-HSMAM1 cells and TC-HSMAM1 cybrids (Fig. 4B). Exposure to oligomycin A (an inhibitor of F_1F_0 -ATP synthase), rotenone (an inhibitor of complex I), and FCCP (a mitochondrial uncoupler) was used to probe for potential disturbances in $\Delta\Psi_m$ maintenance that could be associated with mtDNA damage. Treatment with oligomycin A and FCCP did not result in statistically significant changes in TMRM fluorescence intensity across all cell lines studied. However, exposure to rotenone led to a 1.34-fold reduction in TMRM fluorescence intensity in TC-HSMAM1 cells compared to THP-1 cells, suggesting impaired complex I function due to the m.15059G>A mutation's effect on complex III of the electron transport chain (ETC). In Cas9-TC-HSMAM1 cells, rotenone exposure caused a degree of mitochondrial membrane depolarization similar to that observed in THP-1 cells, indicating an improvement in complex I function (Fig. 4C). Therefore, we demonstrated that a mutation in the gene encoding a critical subunit of complex III also results in complex I dysfunction in the respiratory chain, which may be closely related to the onset of mitochondrial dysfunction.

Mitophagy activation in control THP-1 cells, TC-HSMAM1 cybrids, and Cas9-TC-HSMAM1 cells was evaluated by observing the colocalization of mitochondria and lysosomes using confocal microscopy, with MitoTracker Green and LysoTracker Deep Red indicating their respective locations. We examined PINK1-dependent mitophagy, which was triggered

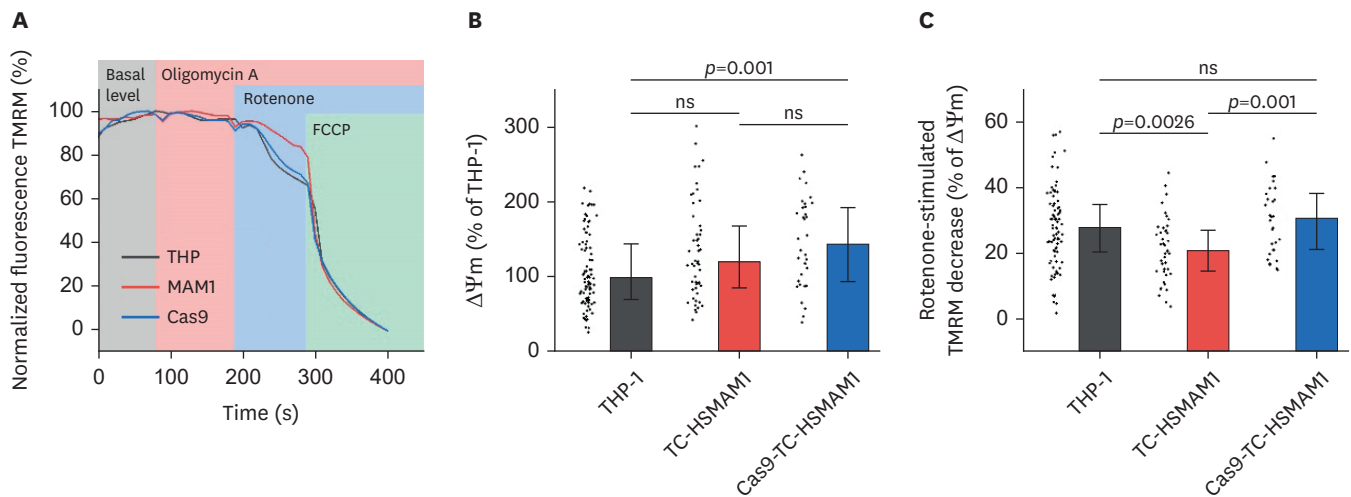


Fig. 4. Elimination of mitochondrial DNA containing the m.15059G>A mutation led to an increase in $\Delta\Psi_m$ and the role of the ETC complex I in $\Delta\Psi_m$ maintenance, as determined by the change in TMRM fluorescence intensity. (A) Tracking of mitochondrial TMRE fluorescence in THP-1, TC-HSMAM1, and Cas9-TC-HSMAM1 cells. (B) Percent change of $\Delta\Psi_m$ in THP-1, TC-HSMAM1, and Cas9-TC-HSMAM1 cells. (C) Percent change of rotenone-stimulated $\Delta\Psi_m$ in THP-1, TC-HSMAM1, and Cas9-TC-HSMAM1 cells. Data information: bars are mean \pm standard deviation. ns ($p > 0.05$), $p = 0.001$, $p = 0.0026$ (Kruskal-Wallis test adjusted with the Bonferroni correction). ns, not significant; $\Delta\Psi_m$, mitochondrial membrane potential; ETC, electron transport chain; TMRM, tetramethylrhodamine methyl ester; FCCP, carbonyl cyanide 4-(trifluoromethoxy)phenylhydrazone; TC-HSMAM1, cybrid cells without transfection with MitoCas9 RNA complex.

by depolarizing the mitochondrial membrane with FCCP, and compared it to the basal mitophagy levels in unstimulated cells. In TC-HSMAM1 cells, FCCP failed to induce a significant change in mitophagy levels (**Fig. 5B**), suggesting that mitophagy was impaired in this cell line.

In contrast, the level of mitophagy increased by 1.39-fold ($p < 0.001$) in FCCP-treated control THP-1 cells (**Fig. 5A**). Similarly, Cas9-TC-HSMAM1 cells treated with FCCP exhibited a 1.38-fold enhancement in mitophagy compared to their basal level ($p < 0.05$) (**Fig. 5C**). Confocal imaging provided further insight into mitophagy activation, revealing the colocalization of mitochondria with lysosomes, which illustrated the dynamics of mitophagy (**Fig. 5D-F**).

To estimate the activation of mitophagy induced by the FCCP-induced depolarization of mitochondrial membranes, we assessed the relative expression of genes involved in the regulation of both canonical (PINK/parkin-mediated pathway) and non-canonical mitophagy (FUN14 domain containing 1 [FUNDC1]-mediated pathway and BCL2 interacting protein 3 [BNIP3]/BCL2 interacting protein 3 like [NIX]-mediated pathway) using real-time qPCR. The genes we examined were *PINK1*, parkin RBR E3 ubiquitin protein ligase (*PRKN*), microtubule associated protein 1 light chain 3 beta (*MAP1LC3B*), *FUNDC1*, *BNIP3* and *NIX*.

Upon FCCP treatment, the THP-1 cells exhibited significant upregulation of *PINK1*, *PRKN*, and microtubule-associated proteins 1A/1B light chain 3B (*MAP1LC3B*) gene expression, confirming the activation of the canonical pathway of mitophagy in these cells (**Fig. 6A-C**). Moreover, the genes related to the non-canonical pathways did not show altered expression in response to FCCP treatment of the THP-1 cells (**Fig. 6D-F**). A similar pattern was observed in the activation of the canonical pathway in the Cas9-TC-HSMAM1 cells: *PINK1*, *PRKN*, and *MAP1LC3B* gene expression increased upon stimulation of mitophagy by FCCP (**Fig. 6A-C**). The only difference is that the *FUNDC1*, *BNIP3*, and *NIX* genes were downregulated in FCCP-treated Cas9-TC-HSMAM1 cells (**Fig. 6D-F**). In contrast, there was no activation of *PINK1* and *PRKN* gene expression upon FCCP treatment of the TC-HSMAM1 cybrid cells (**Fig. 6A and B**). However,

Relationship of mtDNA Mutation With Defective Mitophagy

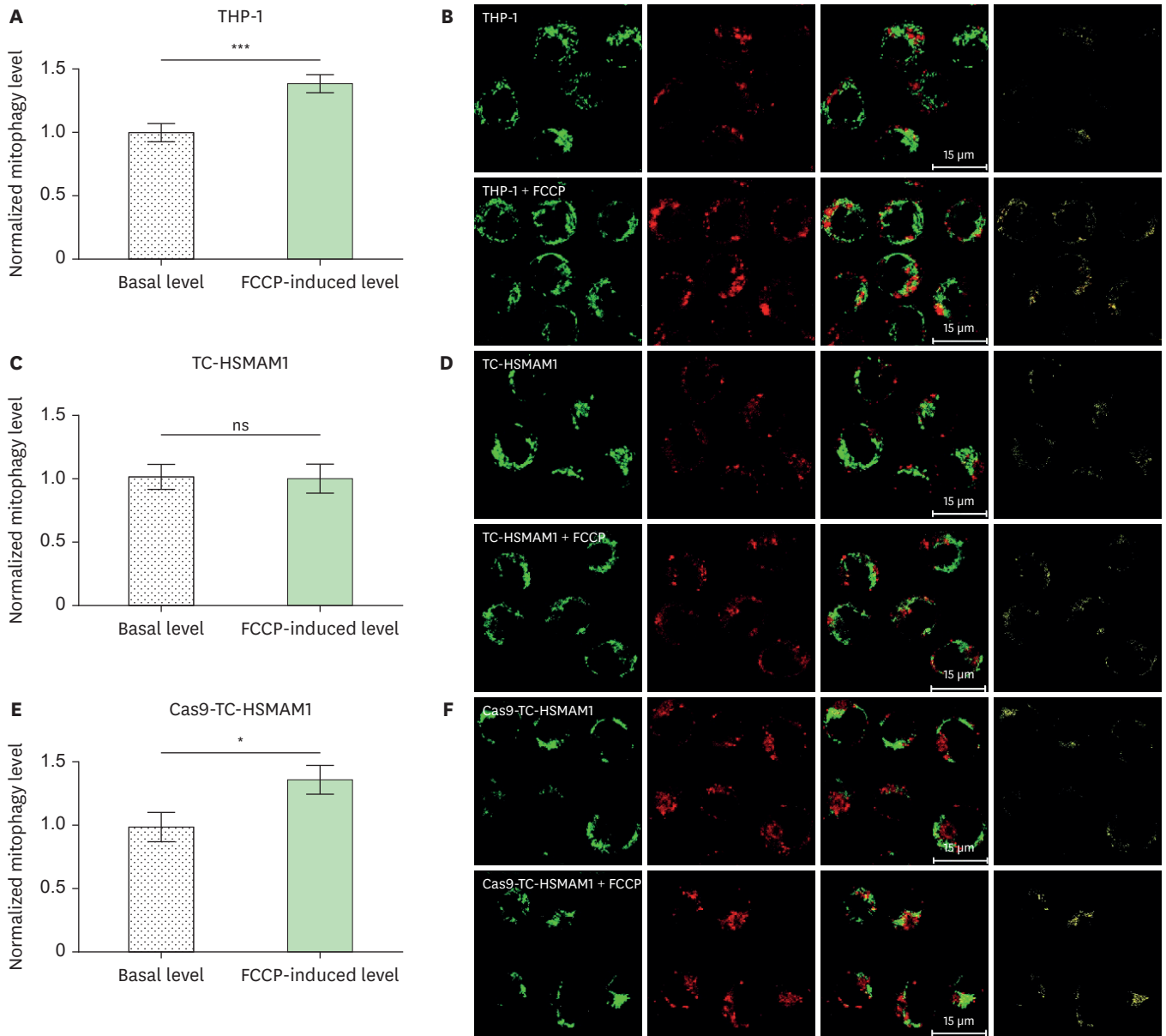


Fig. 5. Mitophagy activity levels in THP-1, TC-HSMAM1, and Cas9-TC-HSMAM1 cells. (A) Normalized mitophagy level in THP-1 cells. (B) Confocal imaging of mitophagy in THP-1 cells. (C) Normalized mitophagy level in TC-HSMAM1 cells. (D) Confocal imaging of mitophagy in TC-HSMAM1 cells. (E) Normalized mitophagy level in Cas9-TC-HSMAM1 cells. (F) Confocal imaging of mitophagy in Cas9-TC-HSMAM1 cells. The level of mitophagy was defined as the number of mitochondria colocalized with lysosomes relative to all mitochondria. Data information: bars are mean \pm standard deviation. Mitochondria were stained with MitoTracker Green dye (green fluorescence), and lysosomes were stained with LysoTracker Deep Red dye (red fluorescence). The channel combination shows the colocalization of lysosomes with mitochondria. Lysosome-enwrapped mitochondria showed as yellow. Magnification $\times 63$. ns, not significant; FCCP, carbonyl cyanide 4-(trifluoromethoxy)phenylhydrazone; TC-HSMAM1, cybrid cells without transfection with MitoCas9 RNA complex. ns ($p > 0.05$), * $p < 0.05$, *** $p < 0.001$ (Student's *t*-test).

TC-HSMAM1 cells treated with FCCP demonstrated a different pattern of expression of *BNIP3* and *NIX* genes compared to Cas9-TC-HSMAM1 cells (Fig. 6E and F). Accordingly, the incubation of TC-HSMAM1 cybrids with FCCP resulted in a statistically significant increase in *MAP1LC3B* and *NIX* expression by 3.32 and 1.42 times, respectively, compared to the basal levels (Fig. 6C and F). However, the expression of *MAP1LC3B* in TC-HSMAM1 cells was significantly reduced compared to Cas9-TC-HSMAM1 cybrids by 3.24 times. Simultaneously, the expression of the *PINK1*, *PRKN*, and *BNIP3* genes in TC-HSMAM1 cybrids did not change

significantly compared to the basal level. Furthermore, the expression of *FUNDC1* in TC-HSMAM1 cybrids was reduced by 13.33 times ($p < 0.001$) upon mitophagy induction with FCCP compared to the basal level (Fig. 6D).

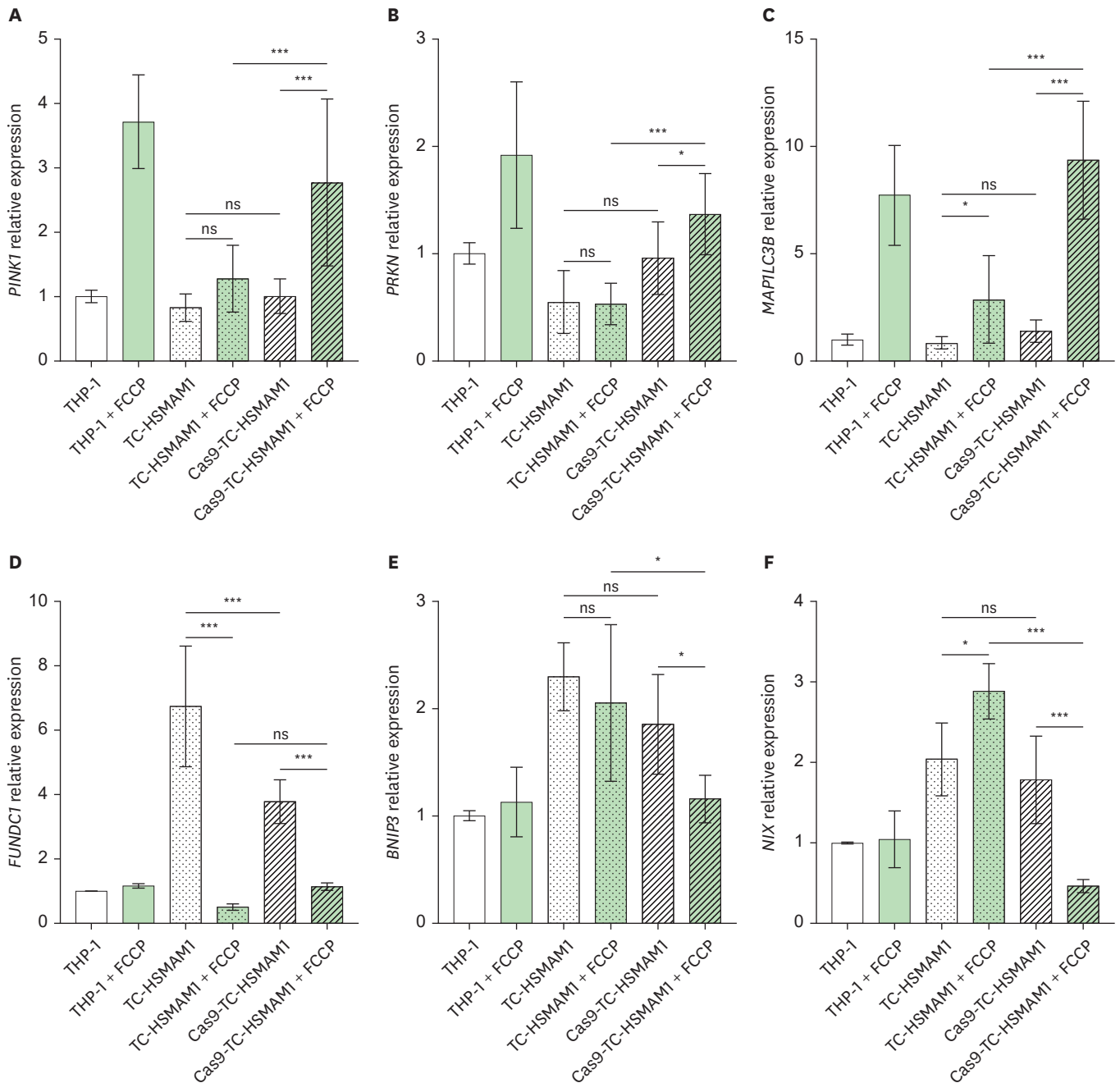


Fig. 6. Evaluation of mitophagy-related gene expression in THP-1, TC-HSMAM1, and Cas9-TC-HSMAM1 cells. (A) Relative expression of the *PINK1* gene. (B) Relative expression of the *PRKN* gene. (C) Relative expression of the *MAP1LC3B* gene. (D) Relative expression of the *FUNDC1* gene. (E) Relative expression of the *BNIP3* gene. (F) Relative expression of the *NIX* gene. Data information: bars are mean ± standard deviation.

ns, not significant; FCCP, carbonyl cyanide 4-(trifluoromethoxy)phenylhydrazone; *PINK1*, PTEN-induced kinase 1; *PRKN*, parkin RBR E3 ubiquitin protein ligase; *MAP1LC3B*, microtubule associated protein 1 light chain 3 beta; *FUNDC1*, FUN14 domain containing 1; *BNIP3*, BCL2 interacting protein 3; *NIX*, BCL2 interacting protein 3 like; TC-HSMAM1, cybrid cells without transfection with MitoCas9 RNA complex.

ns ($p > 0.05$); * $p < 0.05$; *** $p < 0.001$ (one-way analysis of variance adjusted with the Bonferroni correction).

Thus, the elimination of mtDNA carrying the m.15059G>A mutation in cybrid cells led to a significant increase in the expression of the *PINK1*, *PRKN*, and *MAP1LC3B* genes. Our results imply that the m.15059G>A mutation may be associated with the disruption of PINK/parkin-mediated mitophagy processes in monocyte cells. Defective mitophagy, in turn, can lead to the preservation and accumulation of dysfunctional mitochondria in cells, and the aggravation of atherosclerosis.

DISCUSSION

The present study successfully demonstrated the effectiveness of the developed MitoCas9 vector in eliminating mtDNA copies containing the m.15059G>A mutation in the *MT-CYB* gene. Our findings are corroborated by previously reported data from studies utilizing CRISPR/Cas9-based mitochondrial genome editing systems to decrease the targeted mtDNA copy number and levels of its transcripts.¹¹⁴³ Our approach to eliminate mtDNA carrying the m.15059G>A mutation in the *MT-CYB* gene significantly reduced heteroplasmy for this mutation. This allowed us to evaluate the effect of this mutation on the phenotypic and functional properties of the cybrid cells. In addition to TC-HSMAM1 cybrids, we utilized the human monocytic cell line THP-1 as a reference for evaluating the impact of mitochondrial mutations on the functions of cybrid cells obtained from control THP-1 cells. While THP-1 cells and TC-HSMAM1 cybrids have the same nuclear genome, the original cell line cannot serve as a suitable control due to the presence of mitochondria with mtDNA from patients with atherosclerosis, the genetic material of which differs from that of the mitochondria in the THP-1 cell line.^{10,29} Therefore, we evaluated the effect of eliminating mtDNA containing an atherogenic mutation on Cas9-TC-HSMAM1 cells and used the THP-1 cell line as a reference for the macrophage phenotype in a normal physiological condition.

In this study, we utilized the THP-1 cell line, along with the TC-HSMAM1 cybrid cell line and Cas9-TC-HSMAM1 cells, to evaluate cellular parameters. These parameters included the capacity for intracellular lipid accumulation, the production of pro-inflammatory cytokines following LPS stimulation, and mitochondrial function, as indicated by measurements of $\Delta\Psi_m$ and the activation of mitophagy.

The examined mitochondrial mutation was found to have no significant impact on the accumulation of intracellular cholesterol when the cells were incubated with atherogenic LDL. Gene expression analysis revealed that *FASN* was downregulated in Cas9-TC-HSMAM1 cells, suggesting that the m.15059G>A mutation affects the expression of this gene in TC-HSMAM1 cybrids. Consequently, it appears that the m.15059G>A mutation may be linked to alterations in intracellular fatty acid synthesis, even though intracellular cholesterol levels remained unchanged. Numerous studies have indicated a strong correlation between fatty acid synthesis and the development of atherosclerosis.^{30,31} Accordingly, it was reported that the downregulation of the *Fasn* gene in mouse macrophages can contribute to the reduction of atherosclerotic lesions. Moreover, in our previous study, we showed that the m.15059G>A mutation was associated with atherosclerotic lesions in the human aorta.⁸ This finding may partially explain the observed changes in TC-HSMAM1, which include increased *FASN* gene expression compared to both the reference THP-1 cells and the Cas9-TC-HSMAM1 cells. It is well known that macrophage differentiation into foam cells plays a pivotal role in the initial stages of atherosclerotic lesion formation, due to disruptions in intracellular lipid metabolism.³² In turn, the formation of foam cells within atherosclerotic

lesions is thought to be closely linked to mitochondrial dysfunction, which contributes to the disturbance of intracellular lipid metabolism.³³ Therefore, the presence of macrophages harboring atherogenic mtDNA mutations within atherosclerotic lesions could exacerbate the progression of atherosclerosis.

TC-HSMAM1 cybrids were found to be unable to form immune tolerance in response to repeated stimulation with LPS. Immune tolerance is characterized by a reduced immune response in monocytes upon secondary LPS stimulation, which results in decreased cytokine production.³⁴ In the present study, both Cas9-TC-HSMAM1 cells and the original THP-1 cell line exhibited an appropriate response to LPS stimulation. This response was evidenced by an increase in TNF- α secretion following the initial LPS challenge and a reduction in pro-inflammatory cytokine secretion after repeated LPS exposure. The observed effect confirms the development of immune tolerance in human monocytes. Consequently, the m.15059G>A mutation may adversely affect monocyte tolerance, impeding the resolution of inflammation and potentially leading to its chronicity. These findings align with our previous research, which demonstrated a correlation between certain heteroplasmic mtDNA mutations and the pro-inflammatory activation of monocytes in patients with atherosclerosis.³⁵ Furthermore, our results are consistent with data suggesting a possible link between pro-atherogenic mtDNA mutations and the impaired ability of monocytes to establish immune tolerance.⁷

In the assessment of mitochondrial function in the investigated cells, we observed impaired function of complex I in TC-HSMAM1 cybrids following mitochondrial membrane depolarization induced by exposure to rotenone. It is well established that complex I and complex III of the ETC are assembled into a wider supramolecular structure known as the respiratory supercomplex.^{36,37} Consequently, it has been found that a deficiency in complex III, stemming from the presence of nonsense mutations or deletions in the *MT-CYB* gene, coincides with a reduction in the activity of complex I.^{38,39} Recent research has demonstrated the critical role of the C-terminal region of cytochrome b in the regulation of cytochrome b synthesis and the assembly of complex III.⁴⁰ In turn, the m.15059G>A mutation in *MT-CYB* results in the conversion of Gly105 into a stop codon at the C-terminus of cytochrome b, culminating in the formation of a truncated protein.⁴¹ Moreover, complex III is postulated to play a pivotal role in governing the assembly and formation of the supercomplex.³⁶ The dysfunction or loss of complex III due to mutations in *MT-CYB* may impede the assembly of complex I, thereby preventing the incorporation of the NADH module, yet not leading to the degradation of the fully assembled complex I.³⁶ Consequently, the impairment in complex I function that we observed in cells harboring the m.15059G>A mutation in mtDNA is consistent with findings from other studies, indicating a possible onset of mitochondrial dysfunction.

The treatment of cells with FCCP, a mitochondrial uncoupler, can lead to the dissipation of $\Delta\Psi_m$, the production of reactive oxygen species, and other stress signals that activate mitophagy.⁴² We have shown that upon FCCP treatment, cells bearing the m.15059G>A mutation did not show increased expression of the *PINK1* and *PRKN* genes, and the expression level of the *MAP1LC3B* gene was significantly lower than in cells without the m.15059G>A mutation. These 3 genes play a crucial role in the canonical pathway of damaged mitochondria degradation, and downregulation of these genes in TC-HSMAM1 cybrids can decrease the capacity of these cells to degrade damaged mitochondria.^{44,43} The upregulation of *BNIP3* and *NIX* genes in mutant cells may indicate the presence of non-canonical mitophagy in these cells.⁴⁴ However, their activity was insufficient to restore mitophagy upon FCCP treatment, as shown by confocal microscopy.

Our findings indicate that the m.15059G>A mutation can negatively affect PINK1/parkin-mediated mitophagy activation in monocytes, leading to defective mitophagy. It is known that defective mitophagy, caused by the influence of certain agents on cells or mutations in nuclear genes, is accompanied by reduced activity of complex III of the mitochondrial respiratory chain.^{45,46} We hypothesize that in our study, an opposite effect occurred, where the impaired activity of complex III contributed to the reduction of mitophagy activity in cells. Furthermore, a connection between mtDNA mutations and the compromised elimination of dysfunctional mitochondria has been supported by research showing that the m.12338T>C mutation in the mitochondrial gene *MT-ND5* caused a reduction in complex I activity and disrupted mitophagy in cells.⁴ Our data regarding the m.15059G>A mutation's association with the impaired clearance of defective mitochondria in monocytes are consistent with the observed capacity of the cells under study to establish immune tolerance. This provides evidence supporting our theory that defects in cellular immune responses are linked to impaired mitophagy. It should be pointed out that *FASN* may also be involved in LPS-stimulated and Toll-like receptor 4-mediated macrophage activation, leading to increased secretion of pro-inflammatory cytokines.⁴⁷ Consequently, the increased expression of *FASN* may contribute to the increased secretion of TNF- α in response to repeated stimulation of cells with LPS, indicating the inability of cells carrying the m.15059G>A mutation to form immune tolerance.

It is well known that mitophagy is one of the key processes involved in controlling the quality and quantity of mitochondria in cells.⁴⁸ In turn, the close interaction between mitophagy and innate immunity is important for the protective immune response of cells to infectious agents. When cells are exposed to pathogens and inflammation ensues, the innate immune response can influence mitochondrial dynamics and homeostasis, and may also trigger the activation of mitophagy.⁴⁹ It is highly probable that a disruption in the removal of dysfunctional mitochondria could lead to an accumulation of mtDNA mutations, compromised cellular functions, and ultimately, cell death. Conversely, a disruption in autophagy, particularly mitophagy, results in an accumulation of defective mitochondria, which is associated with increased ROS production.⁵⁰ Furthermore, defective mitophagy promotes the hyperactivation of inflammatory pathways, including abnormal inflammasome activation and the subsequent development of chronic systemic inflammation, as well as neurodegenerative, myopathic, cardiovascular, and autoimmune diseases.^{3,51} We have recently shown that modulation of mitophagy in human monocytes can influence the inflammatory response of innate immunity, leading to a decrease in the secretion of pro-inflammatory cytokines. This finding further highlights the close relationship between the degradation processes of defective mitochondria and the development of inflammation.⁷

In summary, the m.15059G>A mutation has previously been shown to be associated with atherosclerotic lesions in the human aorta. In this study, we have determined that the m.15059G>A mutation may be associated with defective mitophagy and the development of chronic inflammation due to the inability of monocytes carrying the mutation to form immune tolerance, as well as with disrupted intracellular lipid metabolism via upregulation of the *FASN* gene. This mutation may play an important role in atherogenesis by potentially contributing to the chronification of inflammation and thereby aggravating the progression of atherosclerosis. The m.15059G>A mutation in the *MT-CYB* gene can be used as a novel genetic marker of predisposition to atherosclerosis in the early stages of the disease. In addition, this mutation may be a potential target for the development of anti-atherosclerotic drugs and therapies.

SUPPLEMENTARY MATERIALS

Supplementary Table 1

Primer sequences for the quantification of the mitochondrial DNA copy number in cybrid cells using digital droplet polymerase chain reaction

Supplementary Table 2

Primer sequences for quantitative real-time polymerase chain reaction analysis of lipid metabolism enzyme gene expression

REFERENCES

- Orekhov AN, Nikiforov NG, Sukhorukov VN, Kubekina MV, Sobenin IA, Wu WK, et al. Role of phagocytosis in the pro-inflammatory response in LDL-induced foam cell formation; a transcriptome analysis. *Int J Mol Sci* 2020;21:817. [PUBMED](#) | [CROSSREF](#)
- Orekhov AN, Nikiforov NG, Omelchenko AV, Sinyov VV, Sobenin IA, Vinokurov AY, et al. The role of mitochondrial mutations in chronification of inflammation: hypothesis and overview of own data. *Life (Basel)* 2022;12:1153. [PUBMED](#) | [CROSSREF](#)
- Gkikas I, Palikaras K, Tavernarakis N. The role of mitophagy in innate immunity. *Front Immunol* 2018;9:1283. [PUBMED](#) | [CROSSREF](#)
- Zhang J, Ji Y, Lu Y, Fu R, Xu M, Liu X, et al. Leber's hereditary optic neuropathy (LHON)-associated ND5 12338T > C mutation altered the assembly and function of complex I, apoptosis and mitophagy. *Hum Mol Genet* 2018;27:1999-2011. [PUBMED](#) | [CROSSREF](#)
- Granatiero V, Giorgio V, Cali T, Patron M, Brini M, Bernardi P, et al. Reduced mitochondrial Ca²⁺ transients stimulate autophagy in human fibroblasts carrying the 13514A>G mutation of the ND5 subunit of NADH dehydrogenase. *Cell Death Differ* 2016;23:231-241. [PUBMED](#) | [CROSSREF](#)
- Cho DH, Kim JK, Jo EK. Mitophagy and innate immunity in infection. *Mol Cells* 2020;43:10-22. [PUBMED](#) | [CROSSREF](#)
- Orekhov AN, Nikiforov NN, Ivanova EA, Sobenin IA. Possible role of mitochondrial DNA mutations in chronification of inflammation: focus on atherosclerosis. *J Clin Med* 2020;9:978. [PUBMED](#) | [CROSSREF](#)
- Sobenin IA, Sazonova MA, Postnov AY, Bobryshev YV, Orekhov AN. Changes of mitochondria in atherosclerosis: possible determinant in the pathogenesis of the disease. *Atherosclerosis* 2013;227:283-288. [PUBMED](#) | [CROSSREF](#)
- Mitrofanov KY, Zhelankin AV, Shiganova GM, Sazonova MA, Bobryshev YV, Postnov AY, et al. Analysis of mitochondrial DNA heteroplasmic mutations A1555G, C3256T, T3336C, C5178A, G12315A, G13513A, G14459A, G14846A and G15059A in CHD patients with the history of myocardial infarction. *Exp Mol Pathol* 2016;100:87-91. [PUBMED](#) | [CROSSREF](#)
- Sazonova MA, Sinyov VV, Ryzhkova AI, Sazonova MD, Khasanova ZB, Shkurat TP, et al. Creation of cybrid cultures containing mtdna mutations m.12315G>a and m.1555G>a, associated with atherosclerosis. *Biomolecules* 2019;9:499. [PUBMED](#) | [CROSSREF](#)
- Hussain SA, Yalvac ME, Khoo B, Eckardt S, McLaughlin KJ. Adapting CRISPR/Cas9 system for targeting mitochondrial genome. *Front Genet* 2021;12:627050. [PUBMED](#) | [CROSSREF](#)
- Bian WP, Chen YL, Luo JJ, Wang C, Xie SL, Pei DS. Knock-in strategy for editing human and zebrafish mitochondrial DNA using Mito-CRISPR/Cas9 system. *ACS Synth Biol* 2019;8:621-632. [PUBMED](#) | [CROSSREF](#)
- Loutre R, Heckel AM, Smirnova A, Entelis N, Tarassov I. Can mitochondrial DNA be CRISPRized: pro and contra. *IUBMB Life* 2018;70:1233-1239. [PUBMED](#) | [CROSSREF](#)
- Carlson-Stevermer J, Abdeen AA, Kohlenberg L, Goedland M, Molugu K, Lou M, Saha K. Assembly of CRISPR ribonucleoproteins with biotinylated oligonucleotides via an RNA aptamer for precise gene editing. *Nat Commun* 2017;8:1711. [PUBMED](#) | [CROSSREF](#)
- Huang X, Yang D, Zhang J, Xu J, Chen YE. Recent advances in improving gene-editing specificity through CRISPR-Cas9 nuclease engineering. *Cells* 2022;11:2186. [PUBMED](#) | [CROSSREF](#)
- Lee J, Jung MH, Jeong E, Lee JK. Using Sniper-Cas9 to minimize off-target effects of CRISPR-Cas9 without the loss of on-target activity via directed evolution. *J Vis Exp* 2019:e59202. [PUBMED](#) | [CROSSREF](#)

17. Lee JK, Jeong E, Lee J, Jung M, Shin E, Kim Y, et al. Directed evolution of CRISPR-Cas9 to increase its specificity. *Nat Commun* 2018;9:3048. [PUBMED](#) | [CROSSREF](#)
18. Chrétien D, Bénit P, Ha HH, Keipert S, El-Khoury R, Chang YT, et al. Mitochondria are physiologically maintained at close to 50 °C. *PLoS Biol* 2018;16:e2003992. [PUBMED](#) | [CROSSREF](#)
19. Shim G, Kim MG, Park JY, Oh YK. Application of cationic liposomes for delivery of nucleic acids. *Asian J Pharm Sci* 2013;8:72-80. [CROSSREF](#)
20. Markov OV, Mironova NL, Maslov MA, Shmendel EV, Zenkova MA. Application of mannose-containing liposomal compositions for obtaining antitumor dendritic cell vaccines. *Biotechnol Med Futur* 2017:75.
21. Butler JM. DNA extraction methods. In: *Advanced topics in forensic DNA typing: methodology*. Elsevier Academic Press; 2012. p.29-47.
22. Sentmanat MF, Peters ST, Florian CP, Connelly JP, Pruett-Miller SM. A survey of validation strategies for CRISPR-Cas9 editing. *Sci Rep* 2018;8:888. [PUBMED](#) | [CROSSREF](#)
23. Orr J, Adamson G, Lindgren F. Preparative ultracentrifugation and analytic ultracentrifugation of plasma lipoproteins. In: Perkins EG, editor. *Analyses of fats, oils, and lipoproteins*. American Oil Chemists' Society; 1993.
24. Havel RJ, Eder HA, Bragdon JH. The distribution and chemical composition of ultracentrifugally separated lipoproteins in human serum. *J Clin Invest* 1955;34:1345-1353. [PUBMED](#) | [CROSSREF](#)
25. Lowry OH, Rosebrough NJ, Farr AL, Randall RJ. Protein measurement with the Folin phenol reagent. *J Biol Chem* 1951;193:265-275. [PUBMED](#) | [CROSSREF](#)
26. Chanput W, Mes JJ, Wichers HJ. THP-1 cell line: an *in vitro* cell model for immune modulation approach. *Int Immunopharmacol* 2014;23:37-45. [PUBMED](#) | [CROSSREF](#)
27. Zaric SS, Coulter WA, Shelburne CE, Fulton CR, Zaric MS, Scott A, et al. Altered Toll-like receptor 2-mediated endotoxin tolerance is related to diminished interferon β production. *J Biol Chem* 2011;286:29492-29500. [PUBMED](#) | [CROSSREF](#)
28. Esteras N, Adjoo-Hermans MJ, Abramov AY, Koopman WJ. Visualization of mitochondrial membrane potential in mammalian cells. *Methods Cell Biol* 2020;155:221-245. [PUBMED](#) | [CROSSREF](#)
29. Tsuchiya S, Yamabe M, Yamaguchi Y, Kobayashi Y, Konno T, Tada K. Establishment and characterization of a human acute monocytic leukemia cell line (THP-1). *Int J Cancer* 1980;26:171-176. [PUBMED](#) | [CROSSREF](#)
30. Schneider JG, Yang Z, Chakravarthy MV, Lodhi JJ, Wei X, Turk J, et al. Macrophage fatty-acid synthase deficiency decreases diet-induced atherosclerosis. *J Biol Chem* 2010;285:23398-23409. [PUBMED](#) | [CROSSREF](#)
31. Chen Y, Wang Z, Xian X, Zhuang Y, Chang J, Zhan X, et al. Eukaryotic initiation factor 6 repression mitigates atherosclerosis progression by inhibiting macrophages expressing Fasn. *IUBMB Life* 2023;75:440-452. [PUBMED](#) | [CROSSREF](#)
32. Sukhorukov VN, Khotina VA, Chegodaev YS, Ivanova E, Soben IA, Orekhov AN. Lipid metabolism in macrophages: focus on atherosclerosis. *Biomedicines* 2020;8:262. [PUBMED](#) | [CROSSREF](#)
33. Lee SJ, Zhang J, Choi AMK, Kim HP. Mitochondrial dysfunction induces formation of lipid droplets as a generalized response to stress. *Oxid Med Cell Longev* 2013;2013:327167. [PUBMED](#) | [CROSSREF](#)
34. Ifrim DC, Quintin J, Joosten LA, Jacobs C, Jansen T, Jacobs L, et al. Trained immunity or tolerance: opposing functional programs induced in human monocytes after engagement of various pattern recognition receptors. *Clin Vaccine Immunol* 2014;21:534-545. [PUBMED](#) | [CROSSREF](#)
35. Orekhov AN, Zhelankin AV, Kolmychkova KI, Mitrofanov KY, Kubekina MV, Ivanova EA, et al. Susceptibility of monocytes to activation correlates with atherogenic mitochondrial DNA mutations. *Exp Mol Pathol* 2015;99:672-676. [PUBMED](#) | [CROSSREF](#)
36. Protasoni M, Pérez-Pérez R, Lobo-Jarne T, Harbour ME, Ding S, Peñas A, et al. Respiratory supercomplexes act as a platform for complex III-mediated maturation of human mitochondrial complexes I and IV. *EMBO J* 2020;39:e102817. [PUBMED](#) | [CROSSREF](#)
37. Lenaz G, Baracca A, Barbero G, Bergamini C, Dalmonte ME, Del Sole M, et al. Mitochondrial respiratory chain super-complex I-III in physiology and pathology. *Biochim Biophys Acta* 2010;1797:633-640. [PUBMED](#) | [CROSSREF](#)
38. Lamantea E, Carrara F, Mariotti C, Morandi L, Tiranti V, Zeviani M. A novel nonsense mutation (Q352X) in the mitochondrial cytochrome B gene associated with a combined deficiency of complexes I and III. *Neuromuscul Disord* 2002;12:49-52. [PUBMED](#) | [CROSSREF](#)
39. Carossa V, Ghelli A, Tropeano CV, Valentino ML, Iommarini L, Maresca A, et al. A novel in-frame 18-bp microdeletion in MT-CYB causes a multisystem disorder with prominent exercise intolerance. *Hum Mutat* 2014;35:954-958. [PUBMED](#) | [CROSSREF](#)

40. Flores-Mireles D, Camacho-Villasana Y, Lutikurti M, García-Guerrero AE, Lozano-Rosas G, Chagoya V, et al. The cytochrome *b* carboxyl terminal region is necessary for mitochondrial complex III assembly. *Life Sci Alliance* 2023;6:e202201858. [PUBMED](#) | [CROSSREF](#)
41. Andreu AL, Bruno C, Dunne TC, Tanji K, Shanske S, Sue CM, et al. A nonsense mutation (G15059A) in the cytochrome *b* gene in a patient with exercise intolerance and myoglobinuria. *Ann Neurol* 1999;45:127-130. [PUBMED](#) | [CROSSREF](#)
42. Ashrafi G, Schwarz TL. The pathways of mitophagy for quality control and clearance of mitochondria. *Cell Death Differ* 2013;20:31-42. [PUBMED](#) | [CROSSREF](#)
43. Kawajiri S, Saiki S, Sato S, Sato F, Hatano T, Eguchi H, et al. PINK1 is recruited to mitochondria with parkin and associates with LC3 in mitophagy. *FEBS Lett* 2010;584:1073-1079. [PUBMED](#) | [CROSSREF](#)
44. Li Y, Zheng W, Lu Y, Zheng Y, Pan L, Wu X, et al. BNIP3L/NIX-mediated mitophagy: molecular mechanisms and implications for human disease. *Cell Death Dis* 2021;13:14. [PUBMED](#) | [CROSSREF](#)
45. Lou Y, Ma C, Liu Z, Shi J, Zheng G, Zhang C, et al. Antimony exposure promotes bladder tumor cell growth by inhibiting PINK1-Parkin-mediated mitophagy. *Ecotoxicol Environ Saf* 2021;221:112420. [PUBMED](#) | [CROSSREF](#)
46. Martín-Maestro P, Sproul A, Martinez H, Paquet D, Gerges M, Noggle S, et al. Autophagy induction by bexarotene promotes mitophagy in presenilin 1 familial Alzheimer's disease iPSC-derived neural stem cells. *Mol Neurobiol* 2019;56:8220-8236. [PUBMED](#) | [CROSSREF](#)
47. Carroll RG, Zasłona Z, Galván-Peña S, Koppe EL, Sévin DC, Angiari S, et al. An unexpected link between fatty acid synthase and cholesterol synthesis in proinflammatory macrophage activation. *J Biol Chem* 2018;293:5509-5521. [PUBMED](#) | [CROSSREF](#)
48. Tan T, Zimmermann M, Reichert AS. Controlling quality and amount of mitochondria by mitophagy: insights into the role of ubiquitination and deubiquitination. *Biol Chem* 2016;397:637-647. [PUBMED](#) | [CROSSREF](#)
49. Zhang L, Qin Y, Chen M. Viral strategies for triggering and manipulating mitophagy. *Autophagy* 2018;14:1665-1673. [PUBMED](#) | [CROSSREF](#)
50. García-Prat L, Martínez-Vicente M, Perdiguero E, Ortet L, Rodríguez-Ubrea J, Rebollo E, et al. Autophagy maintains stemness by preventing senescence. *Nature* 2016;529:37-42. [PUBMED](#) | [CROSSREF](#)
51. Mohanty A, Tiwari-Pandey R, Pandey NR. Mitochondria: the indispensable players in innate immunity and guardians of the inflammatory response. *J Cell Commun Signal* 2019;13:303-318. [PUBMED](#) | [CROSSREF](#)